

A 4D-Var inversion system based on the icosahedral grid model (NICAM-TM 4D-Var)

Niwa, Y.¹, Y. Fujii¹, Y. Sawa¹, Y. Iida², A. Ito³, M. Satoh^{4,5}, R. Imasu⁴, H. Matsueda¹, and N. Saigusa³

1: Meteorological Research Institute (MRI), 2: Japan Meteorological Agency (JMA), 3: National Institute for Environmental Studies (NIES), 4: The University of Tokyo (U. Tokyo), 5: Japan Agency for Marine-Earth Science and Technology (JAMSTEC)

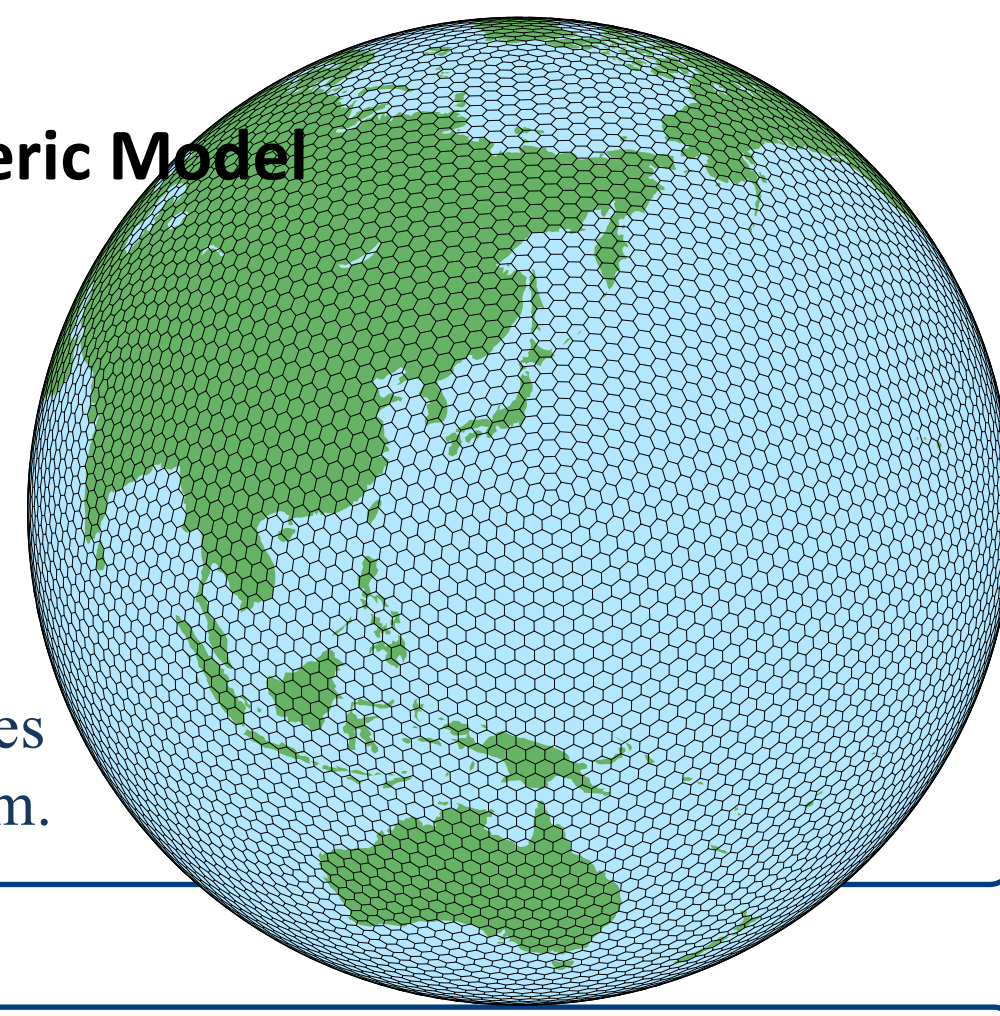
Abstract

Using an icosahedral grid transport model and the 4D-Var method, a new atmospheric greenhouse gas (GHG) inversion system has been developed. Identical twin experiments were conducted to investigate optimal system settings for an atmospheric CO₂ inversion problem in terms of the adjoint models and the optimization schemes as well as to demonstrate the validity of the developed system. Consequently, it is found that a model set of the forward and adjoint models that have less model errors but have non-linearity performs better than another model set that conserves linearity and exact adjoint relationship. Moreover, the effectiveness of prior error correlations was reconfirmed; the global error had reduced by about 15 % by adding prior error correlations that were simply designed. With the optimal setting, the developed inversion system successfully reproduced spatiotemporal variations of the surface fluxes that span from regional anomalies such as biomass burnings to the continental and the global scales. The optimization algorithm introduced in the system does not require any matrix decomposition that is sometimes a difficult task but necessary to consider correlations among the prior flux errors. This enables us to design the prior error covariance matrix more freely. A future study with the developed inversion system and a sophisticated prior error covariance would exploit satellite observations and provide valuable information of GHG flux variation mechanisms.

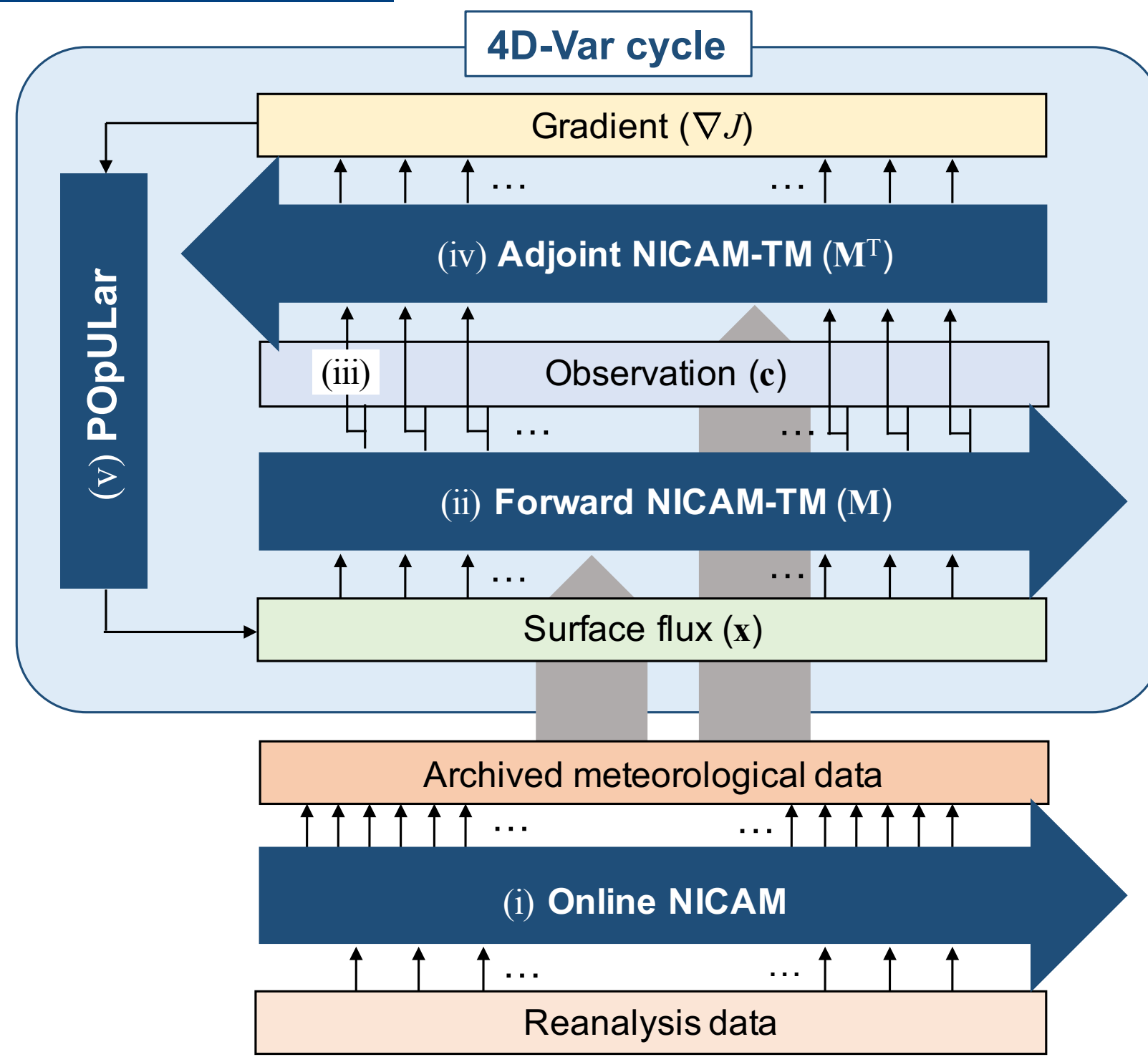
NICAM-TM

Nonhydrostatic Icosahedral Atmospheric Model
(Tomita and Satoh 2004; Satoh et al. 2008, 2014)
-based Transport Model (Niwa et al. 2011)

Owing to the consistency with continuity property, tracer mass is perfectly conserved without any numerical mass fixer, which is favorable for simulations of the long-lived tracers. The off-line forward and adjoint modes of NICAM-TM are used in the 4D-Var system.



4D-Var system



A schematic figure of NICAM-TM 4D-Var

For optimization, we have introduced the scheme of POPULAR (Fujii and Kamachi, 2003; Fujii, 2005). The POPULAR scheme is based on the optimizing scheme of Derber and Rosati (1989) (DR89). Fujii and Kamachi (2003) extended the linear conjugate gradient method of DR89 to non-linear cases using a quasi-Newton method.

The method uses the L-BFGS formula that updates the search direction with an approximated inverse Hessian of \mathbf{H} :

$$\mathbf{H}_{k,-m} = \gamma_k \mathbf{B},$$

$$\mathbf{H}_{k,l} = \mathbf{V}_{k+l}^T \mathbf{H}_{k,l-1} \mathbf{V}_{k+l} + \rho_{k+l} \mathbf{p}_{k+l} \mathbf{p}_{k+l}^T \quad (l = -m+1, \dots, -1, 0),$$

$$\text{where } \mathbf{p}_k = \mathbf{x}_k - \mathbf{x}_{k-1}, \rho_k = 1/\mathbf{y}_k^T \mathbf{p}_k, \mathbf{y}_k = \mathbf{g}_k - \mathbf{g}_{k-1}, \mathbf{V}_k = \mathbf{I} - \rho_k \mathbf{p}_k \mathbf{y}_k^T, \gamma_k = \mathbf{y}_k^T \mathbf{p}_k / \mathbf{y}_k^T \mathbf{z}_k,$$

$$\mathbf{z}_k = \mathbf{B} \mathbf{y}_k = \mathbf{h}_k - \mathbf{h}_{k-1} \text{ and } \mathbf{h}_k = \mathbf{B} \mathbf{g}_k.$$

Then, the search direction can be expressed as a linear combination of \mathbf{h} , \mathbf{z} , and \mathbf{p} as

$$\mathbf{d}_k = -\gamma_k \mathbf{h}_k + \sum_{l=-m+1}^0 (a_{k,l} \mathbf{z}_{k+l} + b_{k,l} \mathbf{p}_{k+l}),$$

where $a_{k,l}$ and $b_{k,l}$ are scalar coefficients that are determined by \mathbf{h}_k and m pairs of \mathbf{p} and \mathbf{z} . It should be noted here that the above equation does not require \mathbf{B}^{-1} calculation. Further to avoid the calculation of \mathbf{B}^{-1} , we here introduce $\mathbf{c}_k = \mathbf{B}^{-1} \mathbf{x}_k$, $\mathbf{q}_k = \mathbf{B}^{-1} \mathbf{p}_k$, and $K_k = \frac{1}{2} \mathbf{x}_k^T \mathbf{B}^{-1} \mathbf{x}_k$. The cost function and its gradient at iteration k are written as

$$J(\mathbf{x}_k) = K_k + \frac{1}{2} (\mathbf{M} \mathbf{x}_k - \mathbf{y}^{\text{dobs}})^T \mathbf{R}^{-1} (\mathbf{M} \mathbf{x}_k - \mathbf{y}^{\text{dobs}}),$$

$$\mathbf{g}_k = \mathbf{c}_k + \mathbf{M}^T \mathbf{R}^{-1} (\mathbf{M} \mathbf{x}_k - \mathbf{d}^{\text{dobs}}).$$

Along with the update of \mathbf{x} by

$$\mathbf{x}_k = \mathbf{x}_{k-1} + \alpha_k \mathbf{d}_k = \mathbf{x}_{k-1} + \mathbf{p}_k,$$

K_k can be also recursively updated as

$$K_k = K_{k-1} + \mathbf{p}_{k-1}^T (\mathbf{c}_{k-1} + \frac{1}{2} \mathbf{q}_{k-1}).$$

Furthermore, \mathbf{c}_k and \mathbf{q}_k can be updated respectively as

$$\mathbf{c}_k = \mathbf{c}_{k-1} + \mathbf{q}_{k-1},$$

$$\mathbf{q}_k = \alpha_k \mathbf{B}^{-1} \mathbf{d}_k = \alpha_k (-\gamma_k \mathbf{g}_k + \sum_{l=-m+1}^0 (a_{k,l} \mathbf{y}_{k+l} + b_{k,l} \mathbf{q}_{k+l})).$$

Practically, POPULAR uses the initial condition of

$$\mathbf{x}_0 = \mathbf{0},$$

$$K_0 = 0,$$

$$\mathbf{c}_0 = \mathbf{0},$$

$$\mathbf{g}_0 = \mathbf{M}^T \mathbf{R}^{-1} (\mathbf{M} \mathbf{x}_0 - \mathbf{d}^{\text{dobs}}),$$

$$\mathbf{h}_0 = \mathbf{B} \mathbf{g}_0,$$

$$\mathbf{d}_0 = -\mathbf{h}_0.$$

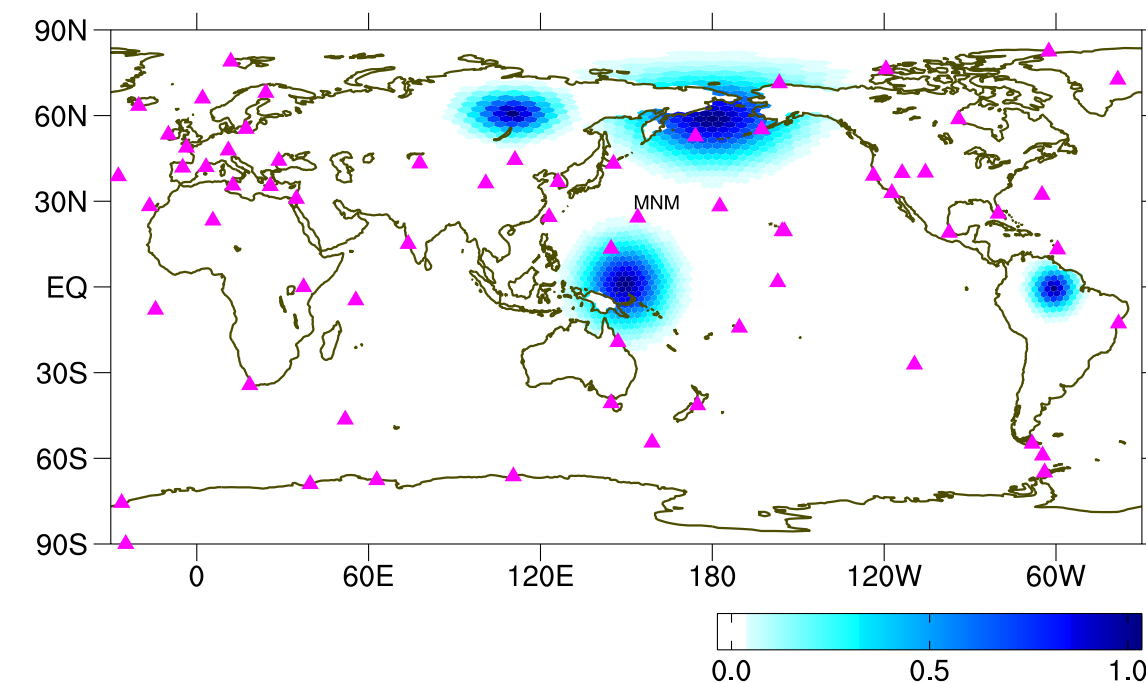
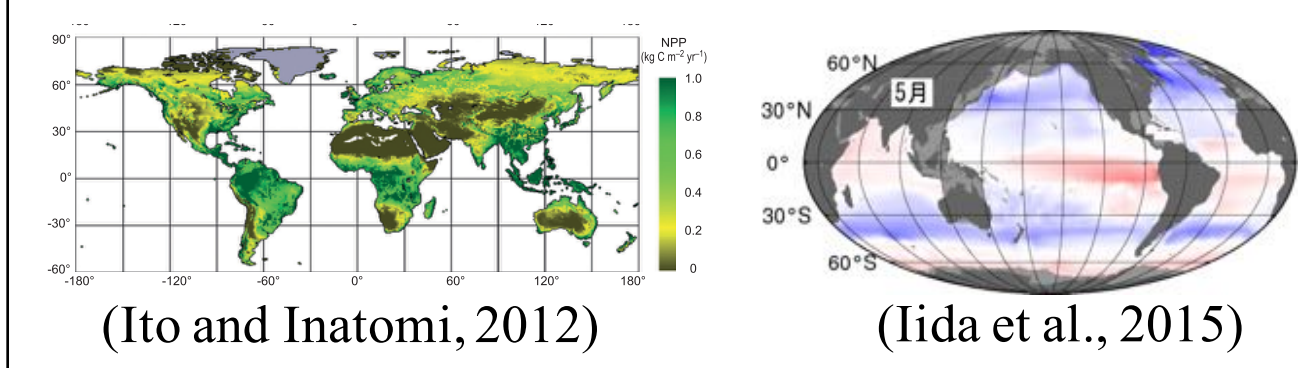
At last, we can see that the sequence of these equations do not require \mathbf{B}^{-1} .

Identical twin experiment

We first run a forward simulation to make pseudo observations using a prescribed flux dataset considered as "true fluxes". In the experiment, a different flux dataset is used as the prior fluxes and the pseudo observations are assimilated into the system to modify the prior fluxes, which is expected to become close to the true fluxes. The validity of the inversion system can be elucidated by evaluating how close the posterior fluxes have reached to the true fluxes after the assimilation. The analysis period, i.e., assimilation window, is set 1 year of 2010 and monthly mean CO₂ fluxes are optimized in the inversion. Therefore, the number of control variables to be optimized is 12 (months) × 10,242 (the number of horizontal grid points) = 122,904. As not optimizing the initial concentrations, we use the same initial concentrations for the true and assimilation runs. We have tested two forward and adjoint model sets: one preserves linearity and complete adjoint relations using the forward model without the flux limiter and the discrete adjoint model (LINEAR) and the other one is a non-linear and non-exact adjoint set using the forward model with the flux limiter and the continuous adjoint model (NON-LINEAR).

Prior fluxes

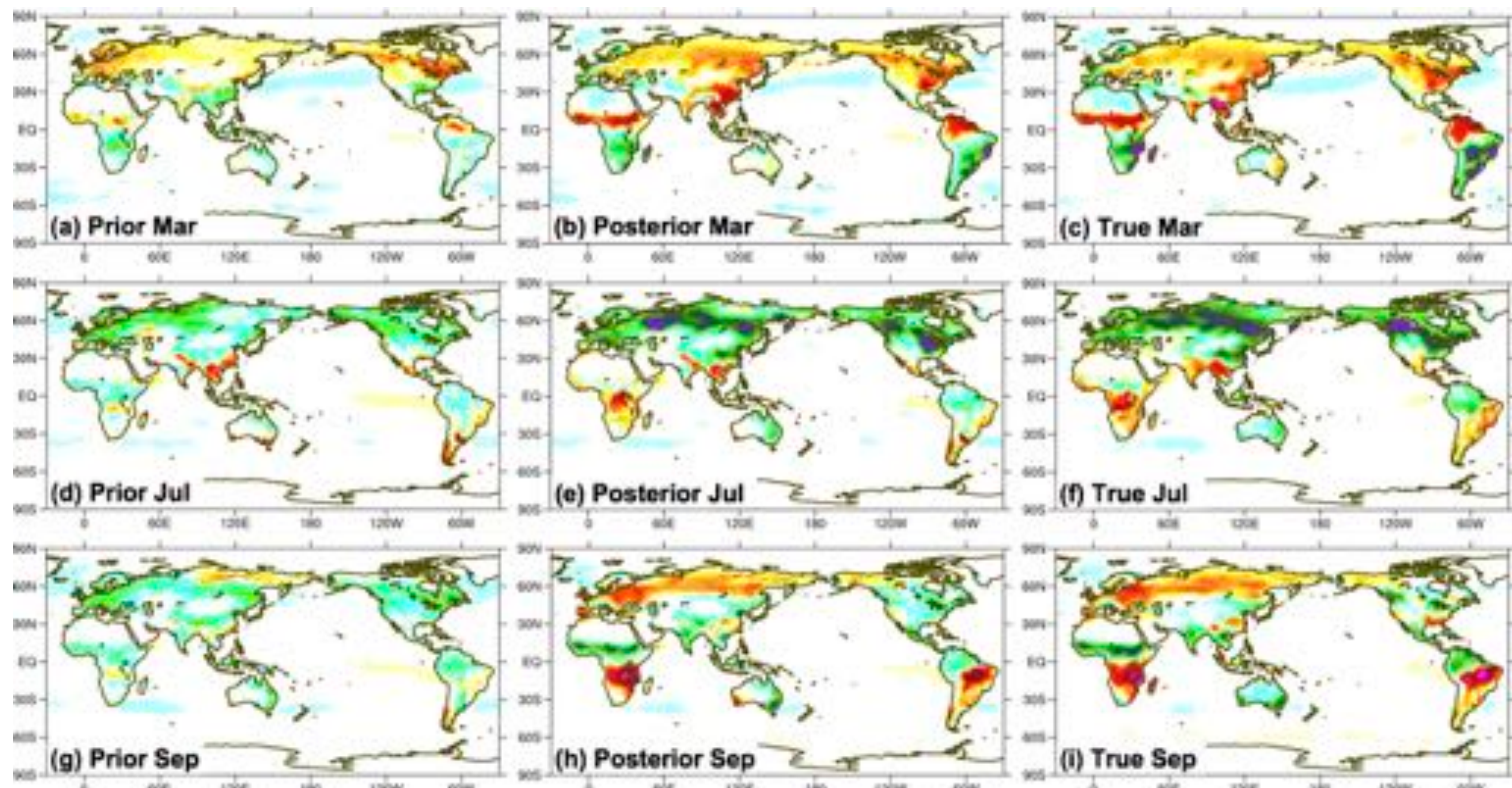
- Terrestrial biosphere flux of VISIT (Ito and Inatomi, 2012)
- Air-sea flux of JMA (Iida et al., 2015)
- Fossil fuel emission of CDIAC (Andres et al., 2013)



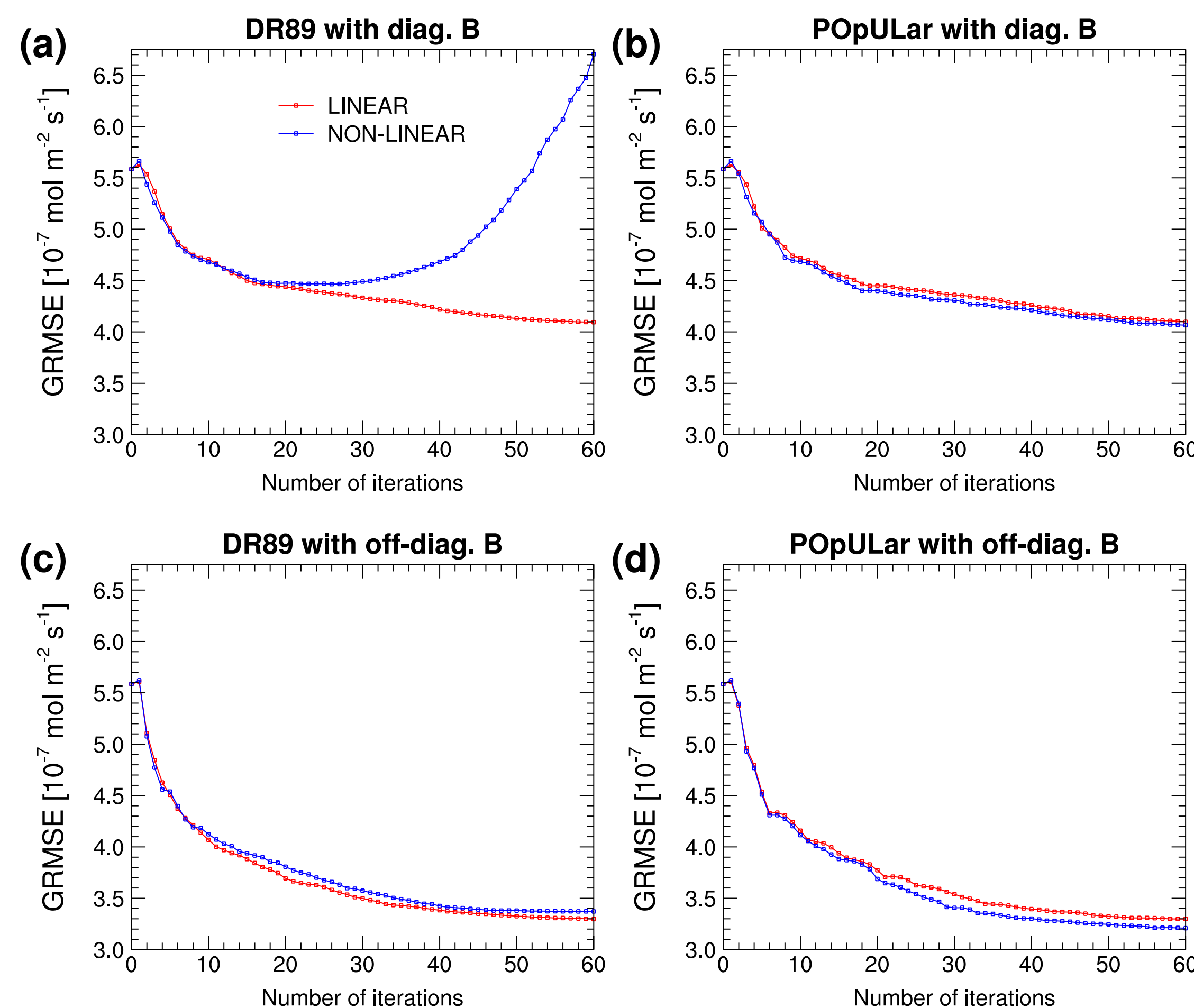
Locations of surface flask observation site (magenta triangle) and four distributions of error correlation introduced in the off-diagonal elements of \mathbf{B} .

True fluxes

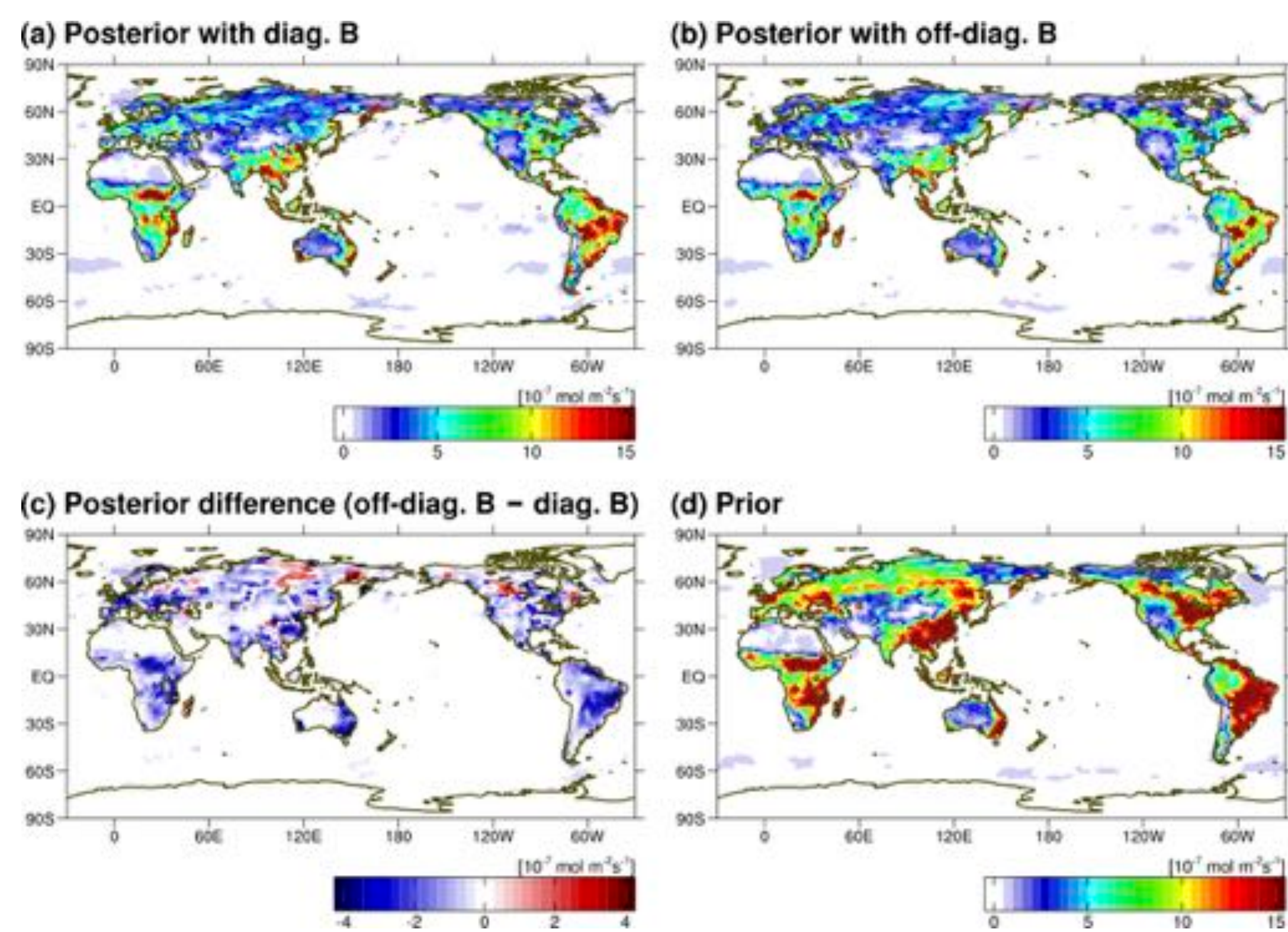
- Terrestrial biosphere flux of CASA (Randerson et al., 1997) modified by the inversion of Niwa et al., (2012)
- Climatological air-sea flux of Takahashi et al., (2009)
- Biomass burning emission of GFED v3.1 (van der Werf et al., 2010)
- Fossil fuel emission of CDIAC (Andres et al., 2013)



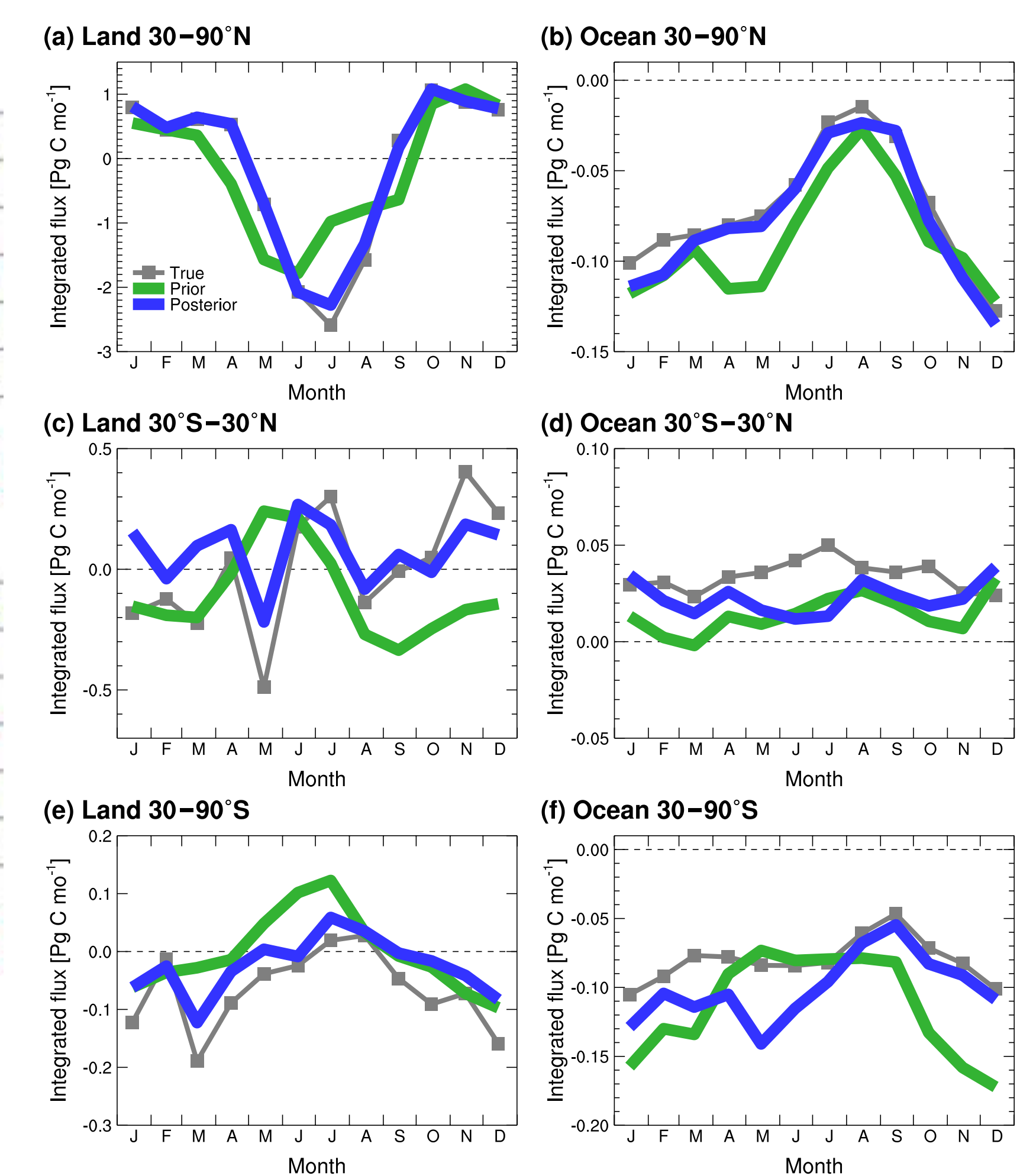
Monthly mean distributions of the prior (left), posterior (middle) and true (right) CO₂ fluxes. Fluxes for three months, March (a-c), July (d-f) and September (g-i) of 2010 are presented. Note that the fluxes do not include fossil fuel emissions, which are not optimized in the inversion.



Global root-mean-square error (GRMSE) changes with iterations for the linear (red) and non-linear (blue) models. Sensitivities to the optimization schemes (DR89: left, POPULAR: right) and to the prior error covariance matrixes (diagonal: upper, off-diagonal: bottom) are evaluated.



Root-mean-square error (RMSE) distributions of the posterior fluxes derived by POPULAR with NON-LINEAR with the diagonal \mathbf{B} (a) and the off-diagonal \mathbf{B} (b). The difference between them (b-a) is also shown in (c) as well as the RMSE distribution of the prior flux (d).



Monthly variations of the true (gray), prior (green) and posterior (blue) CO₂ fluxes integrated for latitude bands of 30–90°N (a,b), 30°S–30°N (c,d) and 30–90°S (e,f). Terrestrial (non-fossil fuel flux) (right) and ocean (left) fluxes are separately shown.

Acknowledgment:

This study is supported by the Environment Research and Technology Development Fund (2-1401) of the Ministry of the Environment, Japan.